16th World Conference on Earthquake, 16WCEE 2017

Santiago Chile, January 9th to 13th 2017

Paper N° 1051

Registration Code: S-B1463214018

Seismic Repair of Severely Damaged Precast RC Bridge Columns Connected with Grouted Splice Sleeves

J.E. Parks[(1)], D.N. Brown[(2)], M.J. Ameli[(3)], C.P. Pantelides[(4)], and L.D. Reaveley[(5)]

[(1)] *PhD Candidate, University of Utah, joel.parks@utah.edu*
[(2)] *Bridge Engineer, Michael Baker International, dylan.neil.brown@gmail.com*
[(3)] *PhD Candidate, University of Utah, m.ameli@utah.edu*
[(4)] *Professor, University of Utah, c.pantelides@utah.edu*
[(5)] *Professor Emeritus, University of Utah, larry.reaveley@utah.edu*

Abstract

A repair technique for severely damaged precast reinforced concrete (RC) bridge columns with grouted splice sleeve (GSS) connections has been developed that utilizes a carbon fiber-reinforced polymer (CFRP) shell and epoxy anchored headed bars to relocate the column plastic hinge. Four original specimens were built using an Accelerated Bridge Construction (ABC) technique with two different GSS systems and were tested to failure using cyclic quasi-static loads. One GSS system was used to connect a precast RC bridge pier cap to a precast column. This GSS system consists of mild steel bars that are threaded into the sleeve at one end and grouted at the other. The second GSS system consists of mild steel bars that are grouted at both ends of the sleeve and is used to connect a RC footing and a precast column. Failure of the four original specimens occurred at drift ratios between 5.6% and 8.0% with longitudinal bar fracture or pullout from the GSS connections. Structural components with this type of damage usually require replacement. However, using the repair method developed, repair of precast RC columns connected using GSS with severe damage is possible.

The damaged plastic hinge of the columns was repaired by increasing the column cross section from a 53 cm octagonal section to a 76 cm diameter circular section over a column length of 46 cm. The repair was constructed using prefabricated CFRP shells to provide confinement and also act as concrete formwork. Inside the prefabricated CFRP shells, headed mild steel bars were epoxy anchored into the pier cap and footing to increase the flexural capacity of the plastic hinge region of the damaged columns. Subsequently, nonshrink or expansive concrete was used to fill the void between the original columns and CFRP shells. The use of expansive instead of nonshrink concrete converts the confinement provided by the CFRP shell from passive to active by pre-tensioning the CFRP shell. The repair method successfully relocated the plastic hinge in the original column section adjacent to the repair and was capable of restoring the diminished load and displacement capacity. Results of the tests conducted on the repaired column assemblies in terms of load capacity and displacement ductility are presented and compared with the original.

Strut-and-tie models (STM) were also developed for the original and repaired precast RC bridge specimens. Generic modeling parameters were established for the STM procedure, enabling the models to be adapted to new repair applications. Special attention is focused on the struts within the CFRP shell. All specimens were modeled using sectional analysis using the predicted STM load to estimate a bilinear force-displacement response envelopes; these predictions show satisfactory agreement with the experiments of the original and repaired bridge specimens in terms of initial stiffness, lateral load and displacement capacity. The repair method is a viable and cost-effective technique for rapid seismic repair of severely damaged precast bridge assemblies.

Keywords: Seismic, Repair, Plastic Hinge Relocation, Strut-and-Tie, FRP Composite

1. Introduction

Repair of severely damaged bridge elements following an earthquake is an advantageous alternative to replacement; the benefits include cost savings, reduction in construction time and decreased interruption for emergency services and the general public. The objective of bridge repair is to rehabilitate damaged bridge elements to a performance level similar to their original performance by restoring the load and displacement capacity of the system. Capacity based bridge design directs damage to bridge columns, thus protecting the pier caps and footings; hence, the post-seismic repair studied is focused on column repair. Repair techniques for damaged bridge columns include the use of externally bonded carbon fiber-reinforced polymer (CFRP) jackets [1], steel jackets [2] and concrete jackets [3]. However, until recently it has been assumed that when longitudinal bars within the column buckle or fracture the column should be replaced [4].

Accelerated Bridge Construction (ABC) is gaining acceptance because of reduced construction time and minimal traffic interruption. Grouted Splice Sleeves (GSS) have been gaining attention as a possible precast concrete connection method for ABC in seismic regions. Researchers are currently investigating the performance of GSS connections for bridges built in seismic regions [5-7]. The use of GSS connections in moderate to high seismic regions is imminent and a practical post-earthquake repair is needed to accompany this new technology. Findings from the current ABC research indicate that columns connected using GSS connectors concentrate the column damage and decrease the effective plastic hinge length compared to traditional monolithic construction, especially if GSS connectors are incorporated in the column ends [8]. These damage characteristics are advantageous for repair purposes, leaving a relatively undamaged column section for plastic hinge relocation.

The repair method developed has been designed and implemented on four severely damaged precast specimens connected using GSS connectors. The specimens had undergone quasi-static cyclic loading reaching a final damage state, before being repaired. The repair uses materials that are available and easy to install including epoxy anchored headed bars, CFRP sheets and nonshrink or expansive concrete. The result is a cost effective, corrosion resistant, rapid repair method which could be installed within a few days. Due to the robust nature of the repair method it is a suitable option for columns of varying damage states, including columns with buckled or fractured longitudinal bars.

Strut-and-tie models (STM) are used to analyze reinforced concrete (RC) members with disturbed internal stress–strain distributions, known as D-regions, to ensure force equilibrium at the ultimate limit state. The STM method is widely accepted in practice [9] and in concrete design codes [10–13]. The STM method is used for cyclically tested precast bridge assemblies; this includes original and repaired bridge assemblies with carbon fiber reinforced polymer (CFRP) shells, headed steel bars, and non-shrink concrete. Techniques previously used for analyzing concrete with CFRP composite jackets [14, 15] and headed steel bars [16] are implemented in the STM models and are used to create a bilinear force–displacement response. The results are compared with the hysteretic curves of two original and two repaired specimens to assess the validity of the STM approach to model repaired concrete assemblies damaged under cyclic loads.

2. EXPERIMENTAL INVESTIGATION OF ORIGINAL SPECIMENS

2.1 Original Test Specimens

Four precast RC specimens representing half-scale bridge elements, conforming to current seismic bridge design standards [17], were constructed utilizing two different GSS systems. Specimens NM-O1 and NM-O2 are column-to-footing assemblies connected with a GSS system which uses high strength nonshrink grout on both ends of the sleeve to splice the bars from the footing and column. Specimens LE-O1 and LE-O2 are column-to-pier cap assemblies connected using a GSS system which uses a threaded connection on one end of the sleeve and a grouted connection on the other. The ID nomenclature for test specimens is as follows: the first two letters represent the splice sleeve type, GSS with both ends grouted is called NM, and GSS with one end threaded and one grouted is called LE; the letter “O” stands for original specimens.

The geometry and reinforcement of the original test specimens is shown in Fig. 1. The columns are 8.5 ft [2.59 m] tall with a 21 in. [533 mm] wide octagonal cross-section. The longitudinal reinforcement consists of

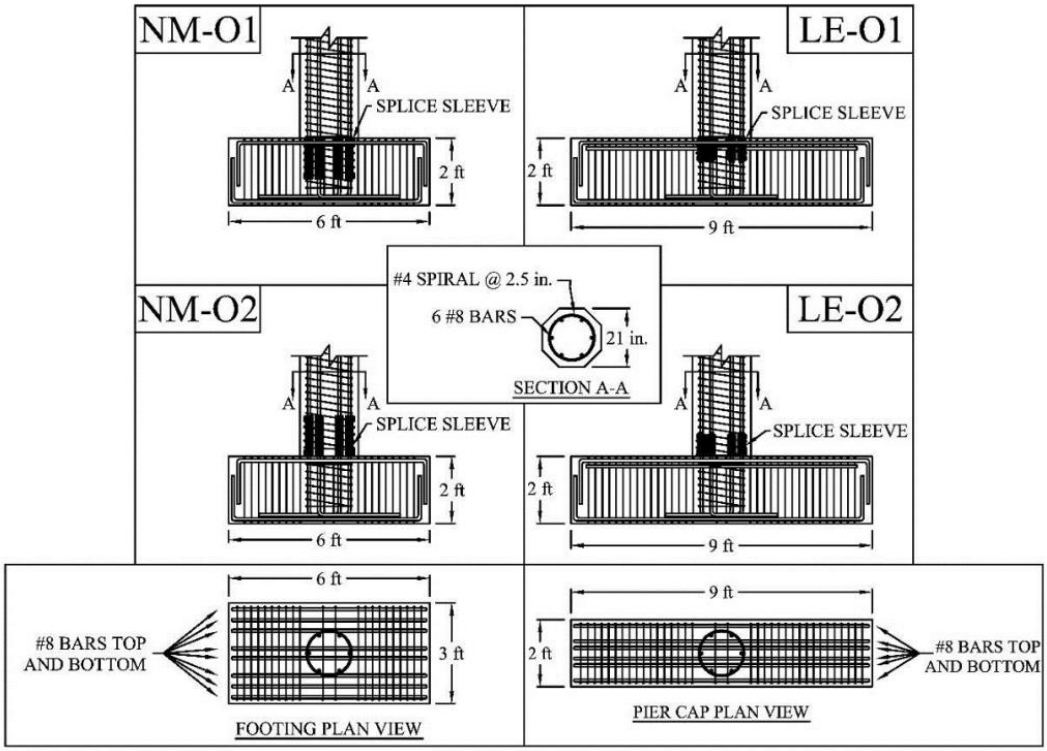

Fig. 1 – Original Specimen Reinforcement and Geometry. *1 ft = 304 mm; 1 in = 25.4 mm.*

6#8 [25 mm] grade 60 [414 MPa] bars arranged in a circular pattern. The GSS connectors are located in the footing and pier cap for NM-O1 and LE-O1, respectively, and in the columns for NM-O2 and LE-O2. A #4 [13mm] grade 60 [414 MPa] spiral at a 2.5 in. [64 mm] pitch is provided for transverse column reinforcement. The footing is 6 ft [1.82 m] long, 2 ft [610 mm] deep and 3 ft [914 mm] wide; the pier cap is 9 ft [2.74 m] long, 2 ft [610 mm] deep and 2 ft [610 mm] wide. The material properties for the precast RC components and the repair are given in Table 1.

In the test assembly, shown in Fig. 2(a), a lateral load is applied at a point that represents the inflection point of a bridge column. The footing and pier cap have spans of 4 ft [1.22 m] and 8 ft [2.44 m] respectively. The pier cap specimen was tested upside down, with the pier cap on the strong floor, for ease of testing. The loading consisted of a constant axial load equal to 6% of the axial load capacity of the column and a displacement controlled cyclic quasi-static lateral load. The lateral load was applied using the loading protocol shown in Fig. 2(b). Two cycles per drift ratio were used and the amplitude was progressively increased until a minimum 20% drop in the lateral load capacity was reached [18].

2.2 Original Test Specimen Results

The damage state of the specimens prior to repair is a critical parameter for the repair design and subsequent performance. The initial test results of NM-O1, NM-O2, LE-O1, and LE-O2 are summarized in Table 2 in terms

Table 1– Material Properties

Material Properties		NM-O1	NM-R1	NM-O2	NM-R2	LE-O1	LE-R1	LE-O2	LE-R2
Longitudinal Bars	f_y, ksi (MPa)	68 (469)	68 (469)	68 (469)	68 (469)	68 (469)	68 (469)	75 (517)	75 (517)
	f_u, ksi (MPa)	93 (641)	93 (641)	93 (641)	93 (641)	93 (641)	93 (641)	103 (710)	103 (710)
Concrete Compressive Strength	Test-Day, ksi (MPa)	5.5 (38)	6.4 (44)	8.4 (58)	9.3 (41)	6.0 (41)	6.1 (42)	8.2 (57)	9.4 (65)

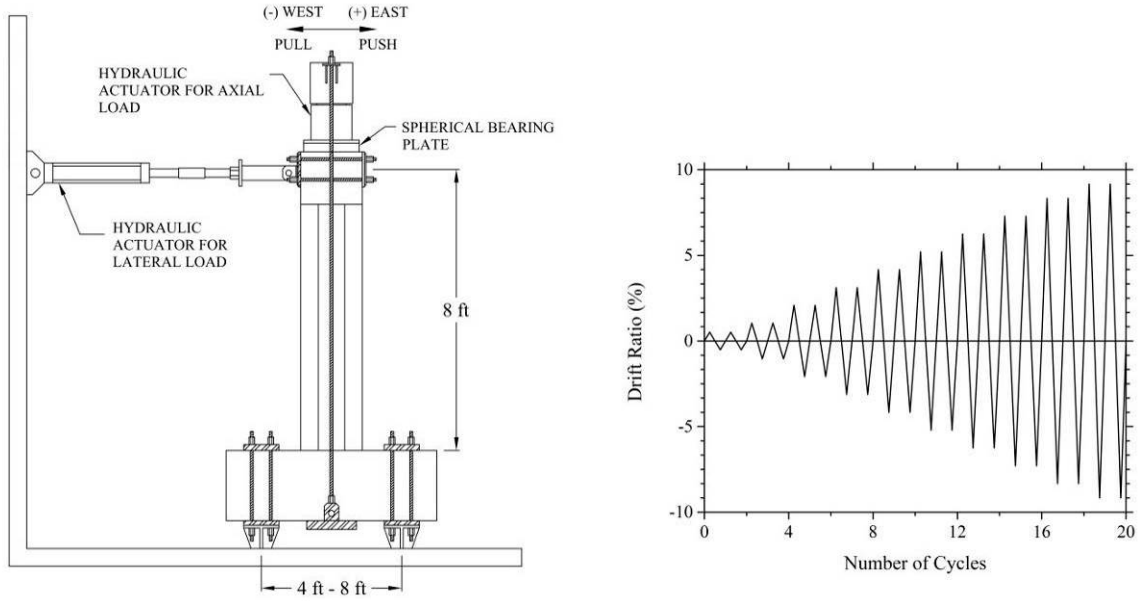

(a) (b)

Fig. 2 – Test Assembly and Loading Protocol: (a) Test Assembly; (b) Loading Protocol. *1 ft = 304mm.*

of maximum lateral load, ultimate drift ratio, displacement ductility, reserve capacity, and failure mode. The failure mode of NM-O1, NM-O2 and LE-O1 was fracture of an extreme longitudinal bar, while LE-O2 failed due to multiple longitudinal bars pulling out from the GSS connections in the column. The extreme east longitudinal bar fractured in both NM-O1 and NM-O2. The extreme west longitudinal bar fractured in LE-O1. At failure of all four original specimens, the lateral load capacity dropped well below 80% of the ultimate load. The reserve lateral load capacity of the original columns after testing ranged from 44% to 65% of the maximum lateral load capacity.

Figure 3 shows the original column damage at the footing-to-column and column-to-pier cap interfaces where extensive spalling and cracking occurred in the plastic hinge region. All original specimens experienced flexural cracking which extended to 14 in. [356 mm] away from the footing or pier cap interface.

3. Repair Procedure

The repair was designed to strengthen the original plastic hinge region, subsequently relocating the plastic hinge to the column section adjacent to the repair. This was achieved by increasing the column cross-section from a 21 in. [533 mm] octagonal section to a 30 in. [762 mm] circular section for a column length of 18 in. [457 mm], as shown in Fig. 4. A detailed description on the design of the repair is presented elsewhere [19].

The first step in the repair procedure was to create a prefabricated CFRP shell. A single layer of 18 in.

Table 2 – Original Specimen Test Results

Test Criteria	NM-O1	NM-O2	LE-O1	LE-O2
Maximum Load, kips (kN)	38.8 (173)	42.0 (187)	36.3 (161)	44.8 (199)
Ultimate Drift Ratio, %	6.69	7.91	6.50	6.00
Displacement Ductility	6.1	6.8	5.8	3.1*
Reserve Capacity, kips (kN)	21.4 (95)	23.6 (105)	20.6 (92)	15.9 (71)
Failure Mode	East Bar Fracture	East Bar Fracture	West Bar Fracture	GSS Bar Pullout

*Value is unnaturally low due to pre-damaged condition before testing [7]

(a) (b) (c) (d)

Fig. 3 – Original Specimen Damage: (a) NM-O1; (b) LE-O1; (c) NM-O2; (d) LE-O2.

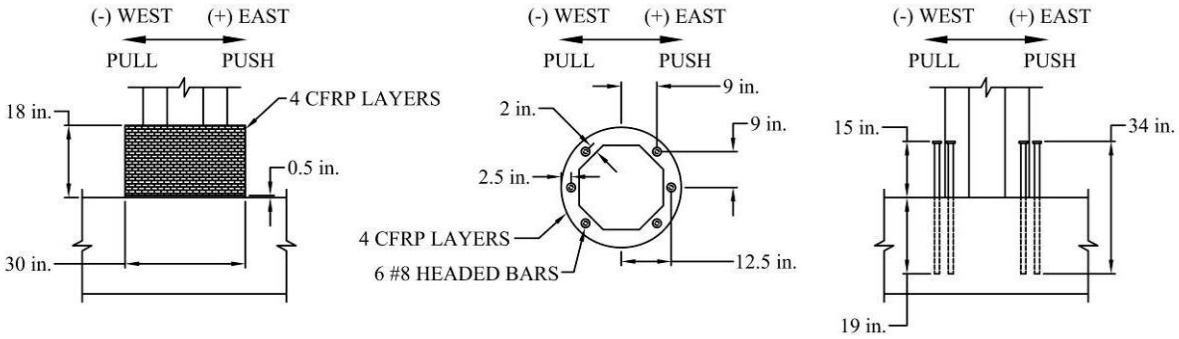

Fig. 4 – Repair Design. 1 in = 25.4 mm.

[457 mm] wide CFRP sheet impregnated with epoxy was wrapped and cured around a 30 in. [762 mm] diameter sonotube to create the proper shape. While the CFRP shell was curing, the holes for the headed bars were core drilled into the footing or pier cap and the headed bars were epoxy anchored into place around the column, as shown in Fig. 5(a). After the CFRP shell had cured it was split in two half cylinders and brought around thecolumn as shown in Fig. 5(b). The splitting and splicing of the first CFRP shell layer was performed to better simulate how the repair would be constructed in the field. A circular shell cannot be lowered over a column since the latter is connected to a footing and pier cap. The sonotube inside the shell in Fig. 5(b) was used to ensure that the shell maintained its shape, while the additional layers of CFRP were applied and was subsequently removed once all CFRP layers had cured. A 12 in. [305 mm] long by 18 in. [457 mm] wide piece of CFRP sheet impregnated with epoxy was used to splice the two halves of the CFRP shell on both sides. Once the first layer of the CFRP shell was spliced, three additional CFRP layers were added as shown in Fig. 5(c). Each layer was 100 in. [2.54 m] long by 18 in. [457 mm] wide, with a 6 in. [152 mm] overlap for each layer. This was the last step in completing the construction of the CFRP shell which acted as stay-in-place formwork for the repair concrete. Once the CFRP shell had fully cured, nonshrink or expansive concrete was added to the space between the column and CFRP shell as shown in Fig. 5(d).

(a) (b) (c) (d)

Fig. 5 – Repair procedure: (a) post installed headed bars; (b) split CFRP shell; (c) CFRP shell around column; (d) CFRP shell filled with nonshrink or expansive concrete.

4. Experimental Results of repaired Specimens

Since the damage state of all original specimens was similar, the same repair design was used for all specimens. The repair procedure was implemented for NM-O1, NM-O2, LE-O1 and LE-O2 and the repaired specimens are referred to as NM-R1, NM-R2, LE-R1 and LE-R2, respectively, where "R" stands for repaired specimen. The only difference in the repair was the type of concrete used to fill the void between the original column and CFRP shell. This concrete, referred to as the repair concrete, was nonshrink concrete for NM-R1 and LE-R1, and expansive concrete for NM-R2 and LE-R2. The use of expansive instead of nonshrink concrete converts the CFRP shell from providing passive to active confinement. The difference in expansion among the repaired specimens was measured by the amount of pre-tensioning experienced by the CFRP wrap prior to testing.

The test assembly and loading protocol remained unchanged for the original and repaired specimens. The strength and displacement capacity of the damaged bridge columns was restored by achieving the same displacement drift and lateral load as the original specimens. The successful plastic hinge relocation for NM-R1 and LE-R1 is shown in Fig. 6.

The hysteretic response of NM-R1 superimposed with the hysteretic response of NM-O1 is shown in Fig. 7(a). It can be seen from the hysteretic response and Table 3, that NM-R1 achieved an 18% larger lateral load than NM-O1 and had a similar displacement capacity. The failure mode of NM-R1 was fracture of column longitudinal bars in the relocated plastic hinge region.

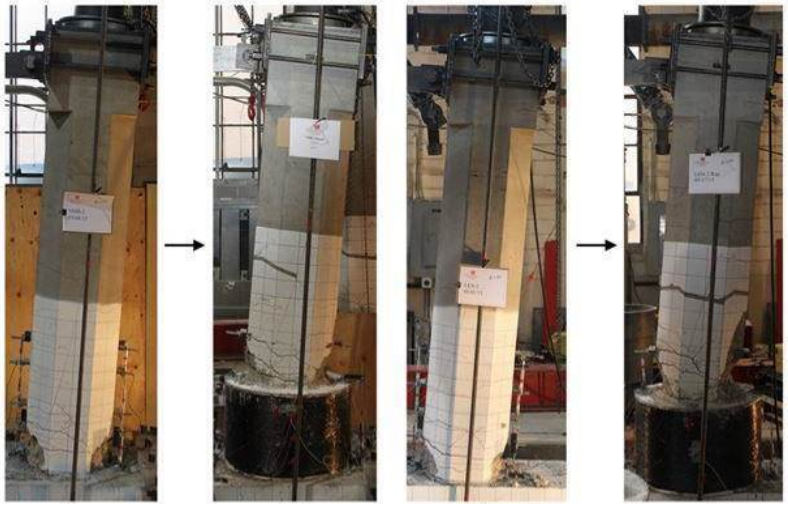

(a) (b) (c) (d)

Fig. 6 – Plastic hinge relocation: (a) NM-01; (b) NM-R1; (c) LE-01; (d) LE-R1.

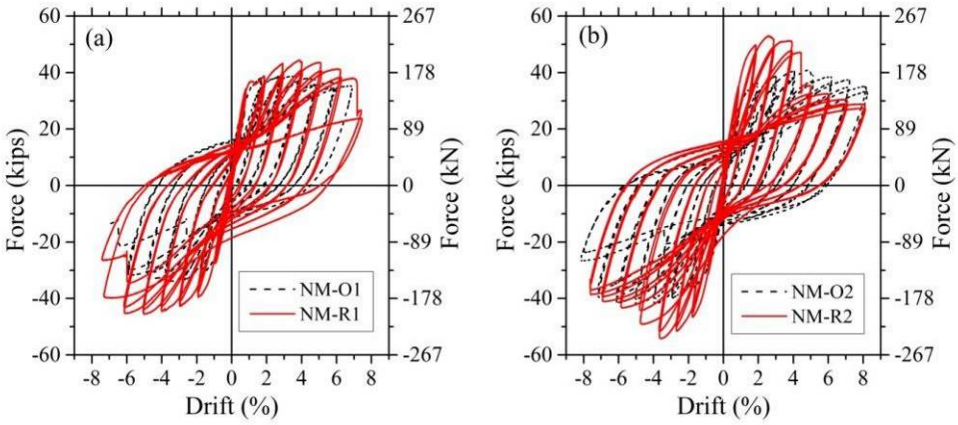

Fig. 7 – NM Hysteretic Response; (a) NM-R1 & NM-O1; (b) NM-R2 & NM-O2

Table 3 – Repaired Specimen Test Results

Test Criteria	NM-R1	NM-R2 (West)	NM-R2 (East)	LE-R1 (Monotonic)	LE-R1 (Cyclic)	LE-R2
Maximum Load, kips (kN)	45.6 (203)	54.2 (241)	53.0 (236)	46.8 (208)	40.5 (180)	50.5 (225)
Ultimate Drift Ratio, %	6.96	5.89	4.60	6.88	7.20	6.17
Displacement Ductility	6.0	3.9	3.9	6.6	---	4.6
Failure Mode	West & East Bar Fracture	West Bar Fracture		---	East Bar Fracture	CFRP Wrap Fracture

]

The hysteretic response of NM-R2 superimposed with the hysteretic response of NM-O2 is shown in Fig. 7(b). The failure mode of NM-R2 was fracture of the extreme west longitudinal bar during the 5.2% drift step. The lateral load capacity of NM-R2 was 28% higher than the lateral load capacity of NM-O2, as shown in Table 3. However, the displacement capacity of NM-R2 was less than that of NM-O2, at the ultimate displacement defined by a 20% drop in lateral load. The longitudinal column bar fracture, which caused the 20% drop in lateral load, was due to embrittlement from welding instrumentation fixtures to the bar. Although a 20% drop in lateral load carrying capacity was observed, the test was carried out through the 8.3% drift step. From the hysteretic response it can be seen that despite the mishap, NM-R2 performed quite well after the column bar had fractured, outperforming NM-O2 in the west direction of testing.

In the case of specimen LE-R1, a monotonic pushover was performed along with the loading protocol of Fig. 2(b). The monotonic load was applied to the column in the east direction until a drift ratio of 6.9% was reached. At this point, the column was brought back to its original vertical position and tested according to the loading protocol of Fig. 2(b). This series of loading emulates a near fault ground motion which is characterized by an acceleration pulse followed by a sinusoidal type ground motion.

The monotonic pushover curve is shown in Fig. 8(a). Although the column was displaced to a drift ratio beyond the ultimate drift ratio of LE-O1, no longitudinal bars fractured in the column due to the monotonic nature of loading. There was major spalling on the east side of the column, as shown in Fig. 6(d) that extended 20 in. [508 mm] up the column and exposed the spiral reinforcement.

With the repaired column already damaged in one direction from the monotonic pushover test, the specimen was subsequently tested cyclically. The hysteretic response of LE-R1 is shown in Fig. 8(a) with the hysteretic response of LE-O1 superimposed. The right side of the hysteresis for LE-R1 shows an irregular response due to damage from the monotonic pushover. The left side of the hysteresis is minimally affected; comparisons of hysteretic response are made to this side of the hysteresis. The failure mode of LE-R1 was facture of the extreme east longitudinal bar in the relocated plastic hinge region. Due to the initial damage of LE-R1 from the monotonic pushover it is difficult to directly compare LE-R1 to LE-O1. However, by examining the

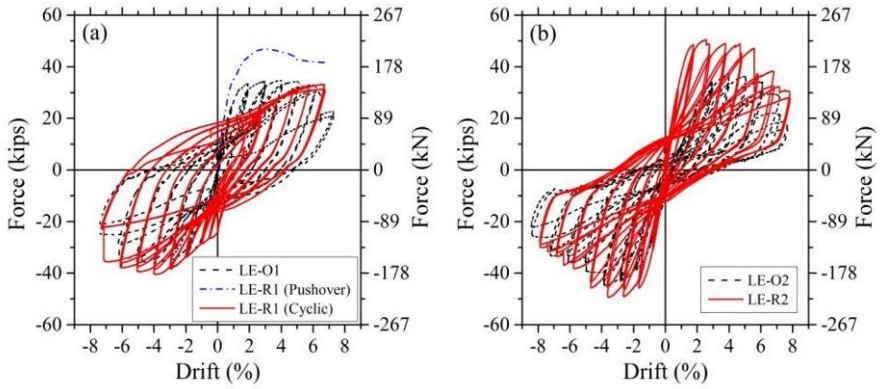

Fig. 8 – LE Hysteretic Response; (a) LE-R1 & LE-O1; (b) LE-R2 & LE-O2.

performance of LE-R1 in Table 3 from both the monotonic pushover and cyclic tests, it is clear that LE-R1 performed similarly to LE-O1.

The hysteretic response of LE-R2 superimposed with the hysteretic response of LE-O2 is shown in Fig. 8(b). During the 3.1% drift step a transverse crack, which correlated with the top of the headed bars, occurred and extended over the entire circumference of the CFRP shell. Before the plastic hinge was completely relocated above the repair, the CFRP shell fractured. Fracture of the CFRP shell occurred during the first cycle of the 6.3% drift step, which caused a 20% drop in the lateral load. This fracture occurred directly below the top of the headed bars and the transverse CFRP crack on the north-east side of the repair. Although a 20% drop in lateral load carrying capacity was observed during the 6.3% drift step, the test was continued through the 8.3% drift step. As the test progressed, the jacket fractured three additional times, with each fracture moving closer to the column pier cap interface.

Although the failure mode of LE-R2 was not the intended one and the plastic hinge was not relocated entirely above the repaired region, the specimen still showed a good hysteretic performance. The lateral load capacity of LE-R2 was 13% higher than the lateral load capacity of LE-O2. However, once the CFRP jacket had fractured, the hysteretic response of LE-R2 followed closely the response of LE-O2.

A more detailed analysis of the all the test results can be found elsewhere [19].

5. Strut-and-Tie Model Formulation

Four STM models were established following ACI 318 [10], for NM-O1, LE-O1, NM-R1 and NM-R2 specimens to predict the ultimate lateral load. Strength reduction factors were not used in the model so comparisons to the test results could be made. The STMs developed are determinate truss models which do not rely on the geometrical or material properties of the members to obtain member forces. Allowable design forces for compression struts and nodes, and tension ties were established following ACI 318 guidelines. The STM procedure outlined within ACI 318 is not intended for modeling lateral force resisting elements. However, due to the conservative nature of STM models, ultimate load prediction matches well the cyclic capacity of the elements; this agrees with previous research findings [20]. The lateral load at which an allowable design force is exceeded for any member within the STM model is the ultimate load capacity of the specimen.

5.1 Strut and Tie Model Layout

Strut-and-tie models require designer input that can only be established through understanding of the stress trajectories within the structure and from experience. This leads to different model layouts from different designers. The present research has established generic parameters to standardize the STM layout of the repaired assemblies, allowing the models to be adapted to new applications in terms of geometry and reinforcement configuration.

The STM layouts developed for all specimens are shown in Fig. 9. The location of external load application within the models was determined based on the experimental configuration. The lateral cyclic load, P_{cy}, is applied to the column in the horizontal direction for each specimen. The vertical axial load, P_{ax}, is applied through external post-tensioned rods into the column and footing or pier cap through bearing plates. The external support reactions in Fig. 9, R_x and R_y, are located where tie down rods were used to secure the specimens to the strong floor, as shown in Fig. 2(a). A more detailed description of all the modeling parameters can be found elsewhere [21].

5.1 Bilinear Force Displacement Response

Bilinear force–displacement models are created to predict the response of the specimens. Each model is created by connecting the effective stiffness of the specimen, computed using elastic beam theory, to the ultimate bending moment predicted by the STM. The ultimate displacement value is determined analytically and from experimental results.

Sectional analysis was applied to predict the effective stiffness of the bilinear force–displacement response curves. Transverse shear deformations were ignored since the shear span-to-depth ratio was large. Bond-slip was

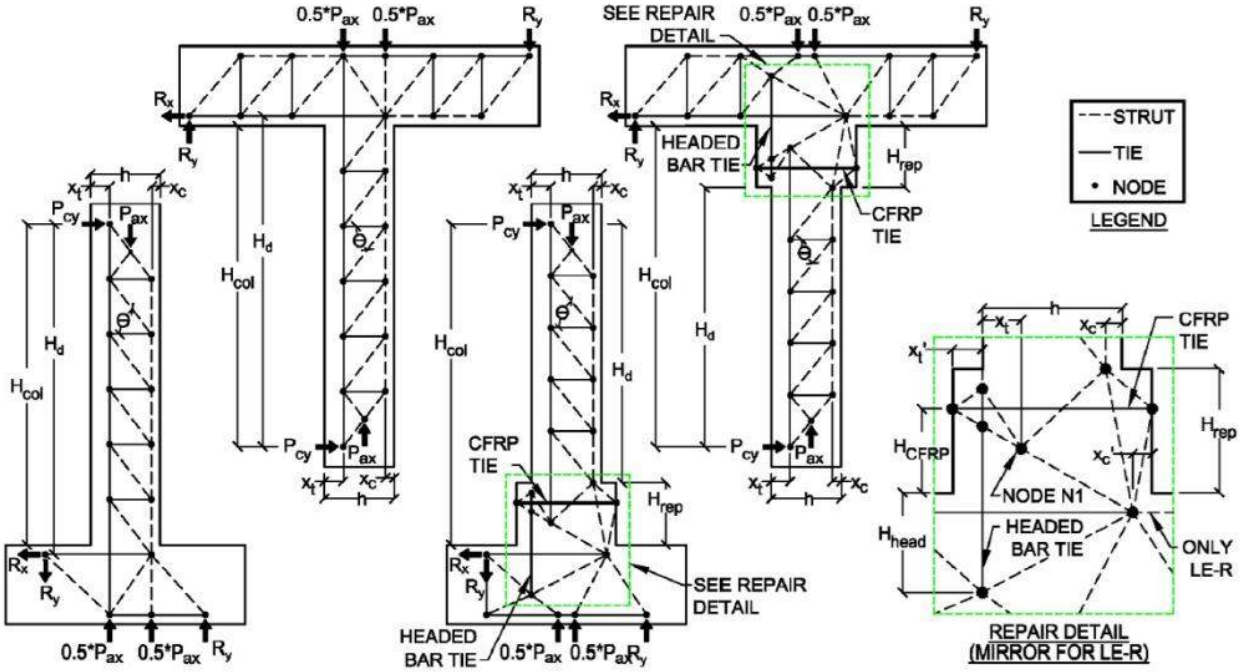

Fig. 9 – STM Model Layout With modeling Parameters: (a) NM-O1; (b) LE-O1; (c) NM-R1; (d) LE-R1; (e) Repair Detail

assumed to have a negligible effect on the stiffness since the method is only valid for the linear portion of the response. The effective flexural stiffness of the original column, EI_{col}, and the repaired region, EI_{rep}, were determined from moment–curvature analysis as:

$$EI_e = M_{yi} / \phi_{yi} \quad (1)$$

where M_{yi} and ϕ_{yi} represent the ideal yield moment and curvature for a bilinear moment curvature approximation. In this study, the bilinear moment curvature approximation follows provisions of bridge design codes [17, 22] where an elastic perfectly plastic response is used to estimate the capacity of the member cross-section.

The effective stiffness of the original column was determined by standard stiffness calculations for a cantilever column in single bending and is defined as:

$$k_{org} = 3EI_{col} / H^3_{col} \quad (2)$$

For the repaired specimen, the effective stiffness was derived to include the effect of a non-prismatic cross-section along a portion of the column and is defined as:

$$K_{rep} = [\ H^3_d / 3EI_{col} + (H^2_{rep} / EI_{rep})(H_{rep} / 3 + H_d + H^2_d / H_{rep})\ ]^{-1} \quad (3)$$

Analytical methods to determine the ultimate displacement of original and repaired precast bridge assemblies connected with grouted splice sleeves is a subject which requires further research. The ultimate displacement of the original precast specimens is taken as the value observed in the tests. The repaired specimens display characteristics which are a closer match to what would be expected of cyclically tested RC monolithic specimens. Therefore two ultimate displacement values are displayed on the bilinear force–displacement response model curves of the repaired specimens: (1) ultimate displacement observed in the tests, and (2) analytical ultimate displacement predicted using monolithic relationships. The analytical ultimate displacement of the system is equal to the product of the displacement ductility, μ_Δ, and yield displacement, Δ_y. This method is discussed further elsewhere [21].

The bilinear force–displacement response model results are compared to the experimental hysteretic responses for specimens NM-R1, NM-O1, LE-R1 and LE-O1 in Figs. 10 and 11. The STM model and experimental results are tabulated in Table 4. The ultimate load predicted by the STM models was 0.95, 0.92, 1.09 and 1.03 times the average ultimate load, for both directions of cyclic testing, for specimens NM-R1, NM-O1, LE-R1 and LE-O1, respectively. These results show very good agreement between STM predictions and experimental results. The ultimate load predicted by the STM was 0.94 times the ultimate load reached during the pushover of LE-R1, showing the excellent correlation of the STM method for both cyclic and monotonic results.

The stiffness values predicted for the four specimens show good correlation to the initial stiffness recorded during testing. When compared to the initial stiffness of the cyclically tested specimens the model predicts 1.32, 1.19, 0.91 and 0.90 times the experimental stiffness observed for specimens NM-R1, LE-R1, NM-O1 and LE-O1, respectively. The over prediction of the model compared to the initial stiffness of specimen NM-R1 and LE-R1 can be attributed to the fact that the repaired specimens experienced significant cracking and plastic deformations in the original test reducing the stiffness.

The ultimate displacement values predicted analytically for specimens NM-R1 and LE-R1 in Fig. 10(c) and (d) under-predict the ultimate displacement observed in the cyclic experiments, as shown in Table 4. The bilinear force–displacement response model compared to the monotonic LE-R1 specimen test shows good agreement, as displayed in Fig. 11. Ultimate displacement relationships for repaired precast bridge assemblies require further research, however the values predicted analytically assuming monolithic properties provide a conservative estimate of the ultimate displacement observed during testing.

6. Conclusions

A method has been developed for post-earthquake repair of severely damaged bridge columns connected using GSS connectors located in the column, footing, and pier cap. The severe damage includes fractured column bars and extensive concrete spalling. The repair converts the original plastic hinge region of the 21 in. [533 mm] octagonal column to a 30 in. [762 mm] diameter circular cross section, thereby relocating the new plastic hinge

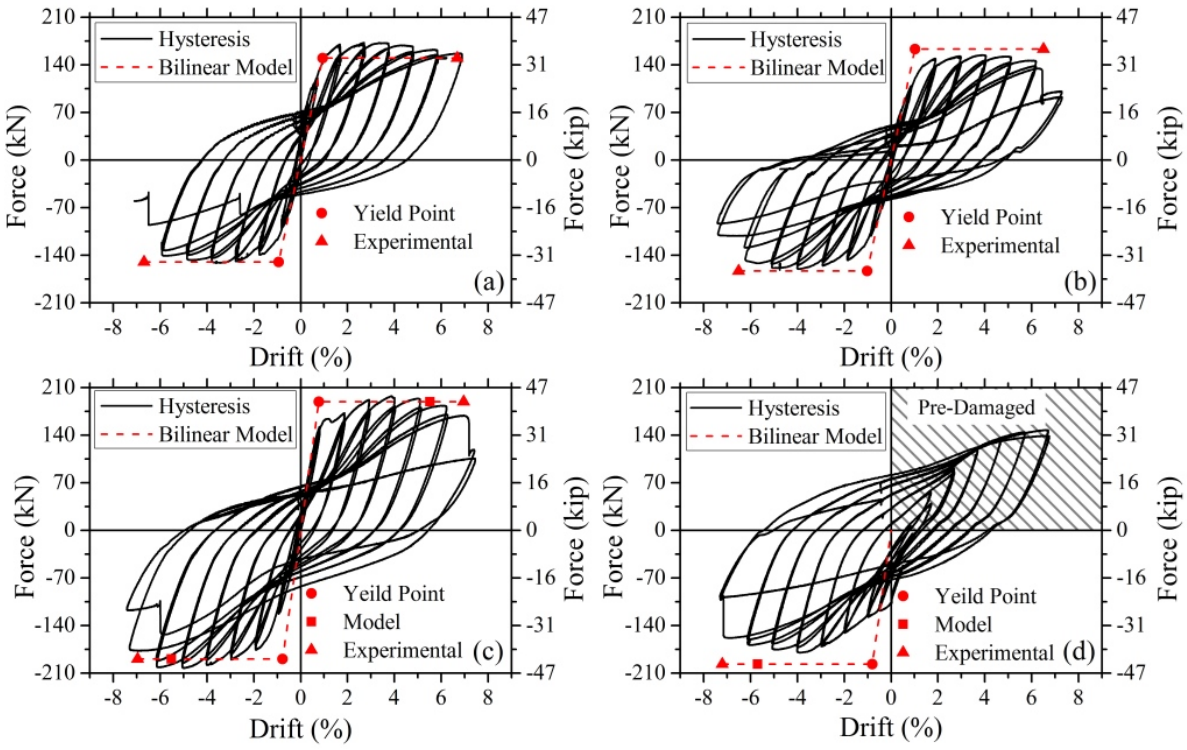

Fig. 10 – Bilinear Force-Displacement Response Model Results Compared to Experimental Response Curves: (a) NM-O1; (b) LE-O1; (c) NM-R1; (d) LE-R1

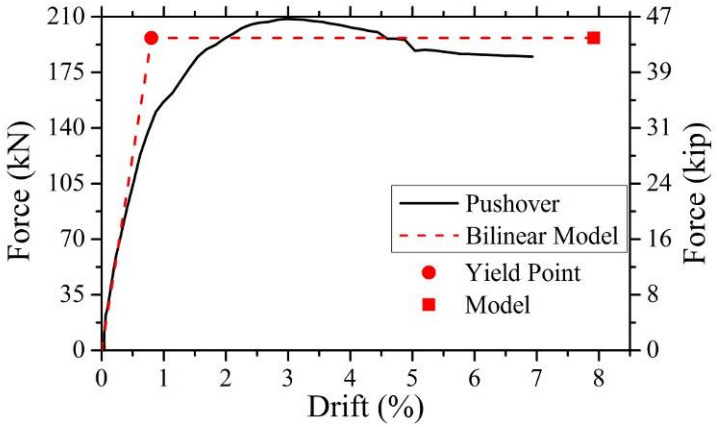

Fig. 11 – Bilinear Force-Displacement Response Model Compared to LE-R1 Pushover Response

Table 4 – Bilinear Force-Displacement Response Model and Experimental Results

Specimen	Ultimate load (kN)			Yield drift ratio (%)			Ultimate drift ratio (%)			Displacement ductility			Initial stiffness (kN/mm)		
	STM	Exp.	STM/exp.	Mod.	Exp.	Mod./exp.	Mod.	Exp.	Mod./exp.	Mod.	Exp.	Mod./exp.	Mod.	Exp.	Mod./exp.
NM-R	189	200	0.95	0.78	1.16	0.67	5.52	6.96	0.79	7.1	6.0	1.19	9.99	7.56	1.32
NM-O	150	162	0.92	0.94	1.10	0.86	–	6.69	–	–	6.1	–	6.53	7.15	0.91
LE-R	197	180	1.09	0.80	–	–	5.70	7.20	0.79	7.1	–	–	10.03	–	–
LE-R PO	197	209	0.94	0.80	1.04	0.77	5.70	6.88	0.83	7.1	6.6	1.08	10.03	8.42	1.19
LE-O	163	158	1.03	1.02	1.12	0.91	–	6.50	–	–	5.8	–	6.54	7.30	0.90

to a minimally damaged section adjacent to the repair. This repair procedure was implemented and tested on cyclically damaged precast bridge column-to-footing and column-to-pier cap assemblies; it was capable of restoring the diminished performance of the specimens in terms of lateral displacement, lateral load, energy dissipation and stiffness.

Based on the overall performance of the repair in the half-scale experiments, this is a viable repair technique for damaged columns in moderate to high seismic regions. In the present case, initial damage of the columns was severe, therefore the method is deemed to be robust and is applicable to columns with varying damage states. The repair technique is rapid and thus satisfies the requirements of accelerated bridge construction.

Strut-and-tie (STM) models have been developed to analyze precast reinforced concrete (RC) bridge assemblies joined with grouted splice sleeves (GSS) both in their original form and after a repair technique using CFRP shells has been employed. The STMs were derived for the specimens following the recommendations of the American Concrete Institute 318. The STM method of analysis was originally developed for monotonic static loads and is not intended to model lateral force resisting elements subjected to cyclic loads; however, the analytical results demonstrate that all four models predicted the unfactored ultimate load capacity of the specimens within 9% of the ultimate cyclic load achieved during the tests. After application of strength reduction factors, all models would provide conservative estimates of the experimental strength of the assemblies, thus proving the design capabilities of the STM method.

Bilinear force–displacement response models were created in this paper to predict the response of the specimens by utilizing their effective flexural stiffness, the ultimate load predicted by the STM method, and the ultimate displacement from displacement ductility considerations. The bilinear force–displacement response models developed extend the STM sectional analysis procedures to provide a simplified alternative to finite-element analysis for finding the response envelope of the original or repaired precast concrete assemblies. The STM models have been developed using adaptable generic modeling parameters, eliminating much designer subjectivity thus facilitating adaption for future applications of the STM method for original and repaired precast concrete assemblies with CFRP shells.

7. References

[1] Seible F, Priestley M, Hegemier G, Innamorato D. Seismic retrofit of RC columns with continuous carbon fiber jackets. Journal of Composites for Construction 1997; 1 (2): 52-62.

[2] Chai Y, Priestley M, Seible F. Seismic retrofit of circular bridge columns for enhanced flexural performance. ACI Structural Journal 1991; 88 (5): 572-584.

[3] Lehman D, Gookin S, Nacamuli A, Moehle J. Repair of earthquake-damaged bridge columns. ACI Structural Journal 2001; 98 (2): 233-242.

[4] Rutledge, S.T.; Kowalsky, M.J.; Seracino, R.; and Nau, J.M., 2014. "Repair of RC bridge columns containing buckled and fractured reinforcement by plastic hinge relocation." Journal of Bridge Engineering; Vol. 19(8), A4013001.

[5] Haber, Z.B.; Saiidi, M.S.; and Sanders, D.H., 2014. "Seismic Performance of Precast Columns with Mechanically Spliced Column-footing Connections." ACI Structural Journal; Vol. 111, No. 3; 639-650.

[6] Ameli, M.J; Parks, J.E.; Brown, D.N.; Pantelides, C.P, 2014. "Grouted Splice Sleeve Connection Alternatives for Precast Concrete Bridge Piers in Moderate-To-High Seismic Regions" Proceedings of the 10th National Confernce on Earthquake Engineering. Anchorage, Alaska.

[7] Ameli, M.J; Parks, J.E.; Brown, D.N.; Pantelides, C.P.,2015."Seismic Evaluation of Grouted Splice Sleeve Connections for Reinforced Precast Concrete Column-to-Cap Beam Joints in Accelerated Bridge Construction." Journal of the Precast/Prestressed Concrete Institute; Vol. 60, No. 2; 80-103.

[8] Pantelides, C.P.; Ameli, M. J.; Parks, J.E.; and Brown, D.N., 2014. "Seismic Evaluation of Grouted Splice Sleeve Connections for Precast RC Bridge Piers in ABC." Utah Department of Transportation Research Division; Report No. UT-14.09.

[9] Sritharan S, Ingham JM. Application of strut-and-tie concepts to concrete bridge joints in seismic regions. PCI J 2003;48(4):66–90.

[10] American Concrete Institute Committee 318. Building code requirements for structural concrete (ACI 318–14) and commentary (318R–14). Farmington Hills, MI: American Concrete Institute; 2014.

[11] American Association of State Highway and Transportation Officials. AASHTO LRFD bridge design specifications. Washington, D.C.: AASHTO; 2012.

[12] International Federation for Structural Concrete, FIB. FIB model code for concrete structures. Berlin: Ernst and Sohn; 2010.

[13] Canadian Standards Association. Design of concrete structures: structures (design)—a national standard of Canada. CAN/CSA Committee A23.3-04. Toronto, ON; 2010.

[14] Saenz N, Pantelides CP, Reaveley LD. Strut-and-tie model for shear friction of concrete with fiber-reinforced polymer composites. ACI Struct J 2004;101 (6):863–71.

[15] Park S, Aboutaha RS. Strut-and-tie method for CFRP strengthened deep beams. J Struct Eng 2009;135(6):632–43.

[16] Hong SG, Chun SC, Lee SH, Oh B. Strut and tie model for development of headed bars in exterior beam column joint. ACI Struct J 2007;104(5):590–600.

[17] American Association of State Highway and Transportation Officials, 2011. "AASHTO Guide specifications for LRFD Seismic Bridge Design." AASHTO ; 2nd edition.

[18] ACI Committee 374. Guide for testing reinforced concrete structural elements under slowly applied simulated seismic loads. ACI 2013; ACI 374.2R-13, Farmington Hills, MI.

[19] Parks, J.E.; Brown, D.N.; Ameli, M.J.; and Pantelides, C.P., 2016 "Seismic Repair of Severely Damaged Precast Reinforced Concrete Bridge Columns Connected with Grouted Splice Sleeves." ACI Structural Journal; Vol. 113, No. 3; 615-626

[20] Barbachyn SM, Kurama YC, Novak LC. Analytical evaluation of diagonally reinforced concrete coupling beams under lateral loads. ACI Struct J 2012;109 (4):497–507.

[21] Brown, D.N.; Parks, J.E.; Ameli, M.J.; Pantelides, C.P., 2016 "Strut-and-tie models of repaired precast concrete bridge substructures with CFRP shell." Composite Structures; Vol. 138; 161-171.

[22] California Department of Transportation, "Seismic Design Criteria." Sacramento, CA: Division of Engineering Services; 2010.